RSC Advances

PAPER

View Article Online
View Journal | View Issue

Cite this: *RSC Adv.*, 2025, **15**, 15832

Facile preparation of environmentally friendly and low-cost thermally responsive microspheres through suspension-emulsion polymerization†

Jinggang Yang, Dongliang Guo, Liheng Yang, Rong Sun and Peng Xiao *

Thermally responsive microspheres (TRMs) have received increasing attention due to their unique temperature-dependent expansion performance. In this work, the preparation of a non-toxic, environmentally friendly, and low-cost TRM was investigated using non-nitrile monomers in suspension-emulsion polymerization. Various TRMs were prepared with different dispersant and emulsifier concentrations, various core materials and polymerization times to study the thermal expansion behavior, thermal response and the mechanism of microsphere polymerization, respectively. The optimized conditions, involving nano-SiO_2 as a dispersant, sodium dodecyl sulfate as an emulsifier, azobisisobutyronitrile as an initiator, as well as styrene, methyl acrylate, methacrylic acid, and methyl methacrylate at a certain mass ratio with a 16-hour reaction time at 65 °C, enabled the production of TRMs with stable spherical structures, high expansion ratios, and smooth, defect-free surfaces. This work provides a facile and environmentally friendly strategy for preparing TRM, which has the potential to be used in industrial applications.

Received 14th February 2025
Accepted 29th April 2025

DOI: 10.1039/d5ra01101a

rsc.li/rsc-advances

1. Introduction

Polymer microcapsules are small containers with a core–shell structure that can encapsulate solids, liquids, or gases within natural or synthetic polymer materials.[1–8] Thermally responsive microspheres (TRMs), as a type of microcapsule material, were first reported in the 1970s and have since seen rapid development.[9–13] TRMs consist of a thermoplastic polymer shell with a low-boiling-point hydrocarbon core.[2,14–16] When TRMs are heated to a specific temperature, the core material vaporizes, creating internal pressure. This pressure causes the microsphere to expand as the shell reaches its glass transition temperature (T_g). At this point, the thermoplastic polymer shell expands under internal pressure, significantly increasing the microsphere's volume while reducing its density. Typically, TRMs can expand to several times their original diameter and up to tens or even hundreds of times their original volume when heated, and these microspheres retain this expanded volume upon cooling.[17,18]

Due to the unique expansion properties, TRMs are widely used as foaming agents or lightweight fillers and are also applied in printing inks to create three-dimensional patterns on paper, wallpaper, and textiles.[19] Moreover, TRMs offer low-pollution and environmentally friendly properties, making them widely utilized in inks,[20] specialty adhesives,[21] colorants[22,23] and novel composite materials.[15,24–32] Current research on TRMs primarily focuses on monomer composition, expansion performance, and applications, while less attention has been paid to the morphological evolution and phase separation behavior during polymerization.[33,34] This gap makes it challenging to prepare microspheres with ideal core–shell structures and optimized expansion properties. Currently, suspension polymerization is a commonly used method for the preparation of physically expandable microcapsules.[35–37] However, studies on the effects of foaming agent types, particle sizes, and dispersants on microcapsule performance remain limited. Traditionally, the preparation of TRMs has relied on monomers such as acrylonitrile (AN) or methacrylonitrile (MAN).[5,35,38–45] AN is toxic, posing environmental and health risks, while MAN is costly, limiting its industrial use. These issues hinder their widespread adoption in large-scale applications. Addressing toxicity and cost remains a challenge for improving industrial processes.[46,47] Recent research efforts have focused on using less toxic and more affordable monomers to partially replace or reduce the use of nitrile-containing monomers.[41,48–53]

In this study, non-nitrile monomers such as methyl acrylate (MA), methyl methacrylate (MMA), and methacrylic acid (MAA) were used as raw materials, with sodium dodecyl sulfate (SDS) as the emulsifier and nano-SiO_2 as the dispersant. A suspension-emulsion polymerization method was employed to prepare thermally responsive microspheres (TRMs), while replacing the toxic acrylonitrile (AN) with styrene (ST). This paper investigates the effects of different dispersant and emulsifier concentrations on microsphere polymerization and

State Grid Jiangsu Electric Power Co., Ltd Research Institute, Nanjing 211103, Jiangsu, P. R. China. E-mail: vodoco@foxmail.com

† Electronic supplementary information (ESI) available. See DOI: https://doi.org/10.1039/d5ra01101a

thermal expansion behavior, examines the influence of various core materials on the thermal response of the microspheres, and explores the impact of polymerization time on TRM preparation conditions to optimize the manufacturing process for TRMs. This work provides a facile and environmental-friendly strategy for preparing TRMs, with the potential to be used in industrial applications.

2. Experimental section

2.1 Materials

Sodium dodecyl sulfate (SDS), methyl methacrylate (MMA), methacrylic acid (MAA), methyl acrylate (MA), styrene (ST), sodium chloride, sodium nitrite and azobisisobutyronitrile (AIBN) were purchased from Aladin Chemical Reagent Co., Ltd (America). SiO_2 (30 nm) was obtained from Qinhuangdao ENO High-tech Material Development Co., Ltd (China).

2.2 The preparation of temperature response microspheres

The temperature-responsive microspheres were prepared according to Scheme 1, following the steps outlined below.

Oil phase: the appropriate amounts of ST, MA, MMA, MAA, AIBN, and alkane (as detailed in Table 1), were mixed thoroughly for later use.

Water phase: 90 mL of deionized water was mixed with a specific amount of SiO_2 and SDS (as listed in Table 1), 1.82 g of sodium chloride, and sodium nitrite (1.53 g, 2.5 wt% water solution). The mixture was stirred until uniform. The amounts of SDS and SiO_2 were based on relevant microsphere studies and validated through preliminary experiments to ensure their suitability.[54]

After combining the oil and water phases, they were mixed at 6000 rpm for 10 minutes using a high-speed stirrer. Then, the mixture was transferred to a three-neck flask and reacted for 16 hours at 65 °C with continuous stirring at 300 rpm under a nitrogen atmosphere, yielding the temperature-responsive microspheres.

2.3 Characterization

The surface morphologies of TRMs were investigated by FEI F-50 field-emission scanning electron microscopy (SEM, America, GB/T 16594-2008). A focused electron beam scans the surface of a sample, and secondary electrons emitted from the sample are detected to produce detailed images of its surface morphology and structure. This method provides high-resolution images for studying the topography, composition, and morphology of materials at the microscopic level. The FT-IR spectra of TRMs were obtained using an Asheville Nicolet-5700 IR spectrometer (America, GB/T 6040-2019). The sample was irradiated with infrared light, and the absorption of specific wavelengths was measured to generate an infrared spectrum. This spectrum can be analyzed to identify functional groups, molecular structures, and chemical bonds present in the sample. The thermal stability testing of TRM was carried out by thermogravimetric analysis (TGA) on a NETZSCH STA 449F5 instrument (Germany). The particle size distribution of TRM was measured using dynamic light scattering (DLS). The method measures the Brownian motion of particles in a solution by analyzing the fluctuations in the intensity of scattered light. Using light scattering theory, the particle's diffusion coefficient is calculated from the frequency variations of the scattered light, which is then used to determine the particle size distribution.

3. Results and discussion

Fig. 1(a) illustrated the synthesis process of the temperature-responsive microspheres. After mixing the oil and water phases, oil phase droplets were formed under the shearing force of high-speed stirring. These droplets remained stable in the water phase due to the dispersing agent. Following AIBN initiation, the polymerization was initiated, resulting in the formation of the temperature-responsive microspheres. As shown in Fig. 1(b), in the 1750–1700 cm^{-1} range, a strong absorption peak was observed, associated with the C=O (ester) stretching vibration in MMA, confirming the incorporation of the ester groups of MMA into the polymer through the polymerization reaction. A characteristic absorption peak was also observed in the 1300–1000 cm^{-1} range, which was related to the C–O bond in ester compounds, further confirming the retention of the ester group in the polymer. Additionally, in the 3000–2800 cm^{-1} range, an absorption peak corresponding to the C–H stretching

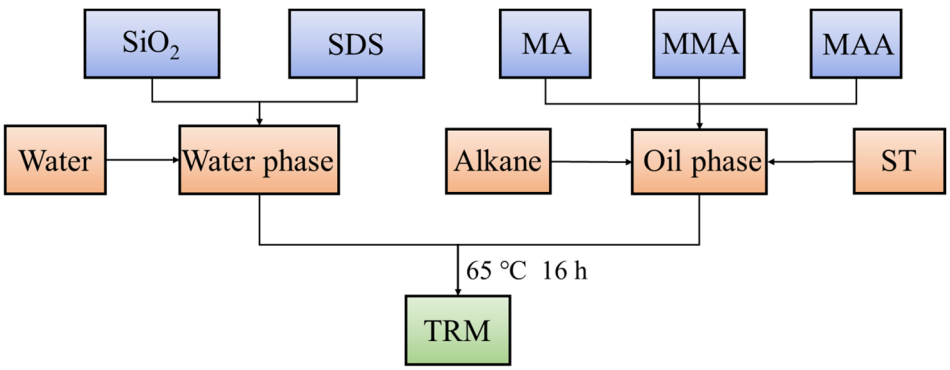

Scheme 1 Preparation process of temperature-responsive microspheres.

Table 1 Detailed formulation for the preparation of temperature-responsive microspheres

Sample	SiO_2 (g)	SDS (g)	ST (g)	MA (g)	MAA (g)	MMA (g)	AIBN (g)	*n*-Octane (g)
TRM-1	1	2	5	5	3	7	0.43	20
TRM-2	2	1	5	5	3	7	0.43	20
TRM-3	2	2	5	5	3	7	0.43	20
TRM-4	2	0	5	5	3	7	0.43	20
TRM-5	0	2	5	5	3	7	0.43	20

vibration of octane was observed, indicating the successful encapsulation of octane in the polymer. The analysis of these characteristic peaks confirmed the typical structural features of the MMA-styrene copolymer in the infrared spectrum and validated the effectiveness of the polymerization reaction. The C═O and C–O peaks provided key insights into the chemical composition of the polymer.

As shown in Fig. S1,† the volume of TRM-1 increased continuously with temperature, while TRM-2 to TRM-5 exhibited almost no change. To further investigate the reasons behind the different volume changes, SEM tests were performed on TRM-1 to TRM-5 both before and after heating.

From Fig. 2(a1)–(e1), it could be observed that the morphology of temperature-responsive microspheres before heating varied significantly across different formulations. The microspheres prepared with the TRM-1 formulation exhibited a complete spherical structure with a smooth surface and no defects, demonstrating excellent granulation and morphological stability. This suggested that the reaction conditions and component ratio in the TRM-1 formulation were favorable for the successful formation of microspheres. In contrast, no spherical structures were observed in the TRM-2 sample, which instead exhibited irregular block-like structures with noticeable aggregation, indicating that this formulation was unsuitable for the stable dispersion and formation of microspheres. The TRM-3 formulation produced a small number of microspheres, but the majority remained as block-like structures. While no significant aggregation was observed, the granulation effect was still suboptimal, possibly due to suboptimal component ratios. In comparison, the TRM-4 sample not only failed to form spherical structures but also exhibited a significantly smaller particle size than TRM-1, suggesting a lower microsphere formation efficiency and limited particle size under these formulation conditions. The TRM-5 sample also failed to form spherical structures and exhibited more pronounced aggregation, indicating poor dispersion performance in this formulation system.

From the post-heating images in Fig. 2(a2)–(e2), it was evident that only the TRM-1 microspheres underwent significant expansion, maintaining an ideal spherical shape. This result indicated that the internal structure of the microspheres was well-designed, encapsulating the alkane core successfully and enabling expansion. In contrast, the TRM-3 microspheres partially expanded; however, most showed surface cracking, indicating structural instability during the expansion. This could result in excessive internal stress, causing the microspheres to rupture and lose the structural integrity. Additionally, there was no expansion in the microspheres from the TRM-2, TRM-4, and TRM-5 formulations. Combining the morphological analysis from Fig. 2(a1)–(e1), it could be concluded that the TRM-2, TRM-4, and TRM-5 microspheres from these formulations did not form spherical structures and failed to encapsulate the alkane core effectively, leading to alkane leakage during heating. Alkane leakage might be the primary reason that these formulations did not exhibit expansion, as the lack of core expansion inhibited the overall expansion of these microspheres.

The polymerization process for preparing temperature-responsive microspheres using AIBN as an initiator could be

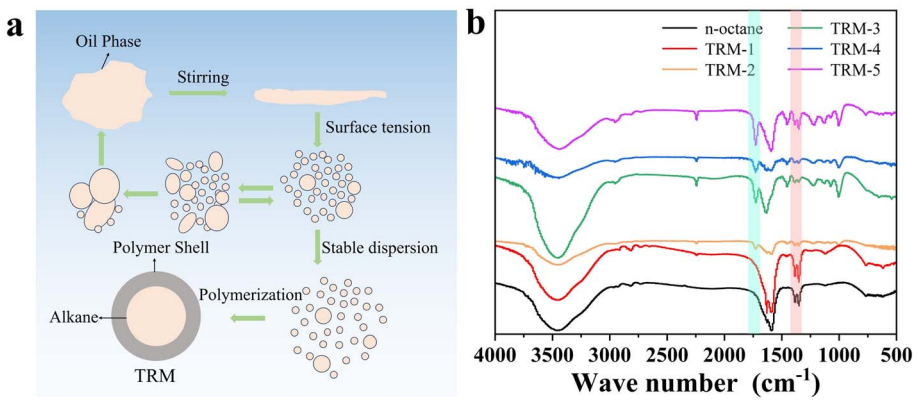

Fig. 1 (a). Schematic illustration of the preparation of temperature-responsive microspheres. (b). FT-IR spectra of temperature-responsive microspheres.

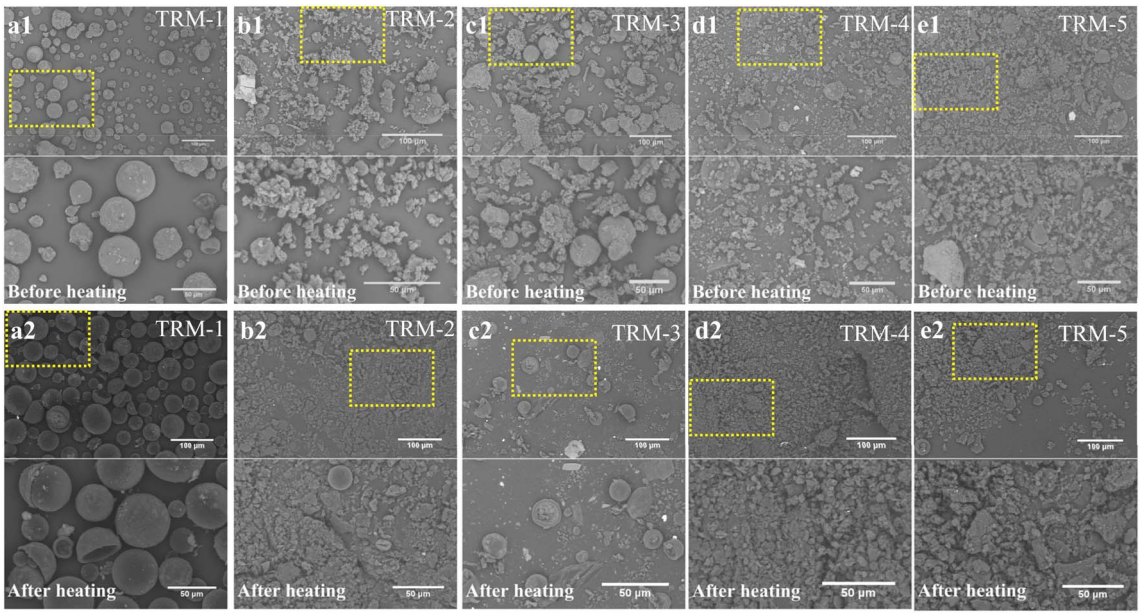

Fig. 2 (a1–e1) SEM images of temperature-responsive microspheres before heating. (a2–e2) SEM images of temperature-responsive microspheres after heating (160 °C).

divided into several stages, which sequentially revealed the mechanisms of alkane and monomer diffusion, nucleation, particle growth, and the eventual formation of a stable core–shell structure. At the early stages of polymerization, alkanes and monomers diffuse from the oil phase into the aqueous phase. AIBN, acting as the initiator, triggered a free radical polymerization reaction at the oil–water interface. At this point, both the alkanes and monomers in the oil phase were in the form of droplets, and readied to provide a reactive environment for subsequent nucleation and polymerization. Nucleation in the aqueous phase was the next crucial step. Small initial nuclei formed in the aqueous phase, providing a core for further particle growth. The nucleation process occurred under the initiation of AIBN and determined the final size and morphology of the microspheres. After nucleation, the monomers adsorbed onto the nuclei, driving continued particle growth. The monomers in the aqueous phase gradually adhered to the initially formed nuclei, enhancing the size and stability of the particles. As the monomers continued to approach and react with the nuclei, the particles began to exhibit significant growth. Over time, particle growth and secondary nucleation processes became evident. The initially formed nuclei were enlarged by gradually adsorbing more monomers, and secondary nucleation might occur, generating new particles. At this stage, polymer chains formed and gradually. Separated from the alkanes and monomers. Subsequently, rapid phase separation occurred as the polymer chains grew and began to envelop the alkanes. A distinct phase separation between the alkanes and the formed polymer arose, with the polymer chains separating from the oil phase and encapsulating the internal alkanes. This step was crucial for the formation of core–shell microspheres, as the effective encapsulation of alkanes was essential for achieving the desired expansion effect. Finally, the reaction progressed to the formation of a stable core–shell structure. As the reaction was completed, the polymer shell fully formed, successfully enclosing the alkanes within the core of the microsphere. At this point, the microspheres exhibited a complete core–shell structure with a smooth, defect-free surface and a uniform particle size distribution. Microspheres were capable of significant volume expansion in subsequent processes, meeting the application requirements. As shown in Fig. 3, the polymerization process in the aqueous phase, initiated by AIBN, underwent nucleation, growth, phase separation, and structural stabilization. The efficient phase separation mechanism in this process ensured the successful expansion of

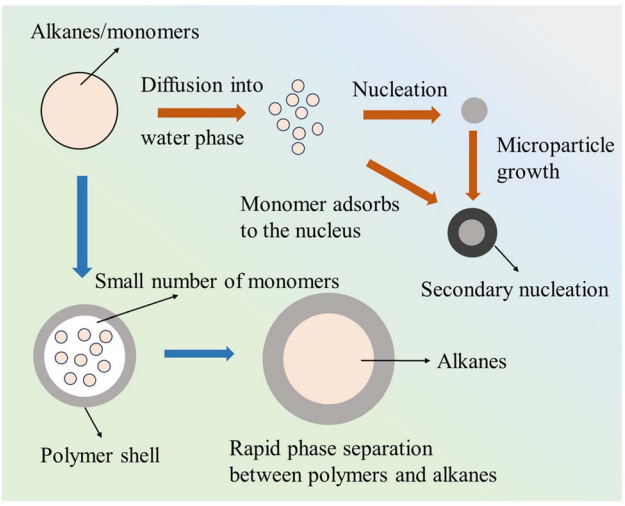

Fig. 3 Schematic diagram of the temperature-responsive microsphere polymerization process.

the microspheres and laid the foundation for future industrial applications.

To investigate the effect of polymerization time on the structure of temperature-responsive microspheres, the TRM-1 formulation from Table 1 was used, with AIBN as the initiator and *n*-octane as the alkane. The polymerization was conducted at 65 °C, with recordings made every 4 hours. The morphological changes of droplets/polymer microspheres during the 16-hour polymerization process were observed, as shown in SEM images in Fig. 4(a)–(d). After 4 hours of polymerization, the particles mainly existed as microparticles, with a clear core–shell interface. The shell layer consisted of the formed polymer solution, and the polymer chains gradually precipitated from the oil phase, undergoing phase separation to form a very thin, discontinuous shell. The core of the particles was occupied by the unreacted monomers and alkane oil phase at the center. As the reaction time was extended to 8 hours, the microparticles began to aggregate and grow, forming larger particles. After 12 hours of reaction, the particle morphology changed significantly, and a spherical structure appeared, indicating that the polymerization had reached the mature stage and microspheres were gradually taking shape. As the reaction continued, AIBN initiated the monomer reaction in the aqueous phase due to the lack of aqueous phase inhibitors, causing MMA to migrate from the oil phase to the aqueous phase, where polymerization occurred. The secondary microparticles that were generated gradually adsorbed onto the surface of the microspheres. At the same time, the migration of monomers from the oil phase and the increasing alkane concentration accelerated phase separation of the polymer, with polymer chains moving to the microsphere surface and gradually merging to form a more stable shell structure. The alkane diffused to the center of the droplets, further concentrating in the microsphere core. After 16 hours of reaction, the microspheres formed a typical core–shell structure (Fig. S5†), with the core composed of alkanes and the shell made of polymer, showing a complete core–shell morphology.

To further explore the impact of polymerization time on microsphere size, particle size analysis was performed, as shown in Fig. 5. The SEM images in Fig. 4 and the particle size distribution graph in Fig. 5 clearly demonstrated that the morphological changes of the microparticles at different reaction times closely correspond with the trend of particle size growth. After 4 hours of reaction, the particle size ranged from 500 nm to 1 μm, indicating that the microparticles were still small and in the early stages of polymerization. At 8 hours, the particle size increased significantly, with most particles ranging from 5 μm to 10 μm. This result indicated that the particles underwent significant aggregation and growth, becoming more stable, and the polymerization reaction promoted further maturation of the particles. After 12 hours, the particle size increased further, with a distribution range extending from 10 μm to 50 μm. The particle morphology became more mature, with the microparticles undergoing sufficient aggregation and polymerization, and the size further increased, indicating that the spherical effect of the particles was gradually reaching its optimal state. After 16 hours of reaction, the particle size stabilized between 10 μm and 50 μm, indicating that particle growth was essentially completed, and the size distribution was uniform, reaching the final morphological state (Fig. S4†). This result showed that a 16-hour reaction time was sufficient for the microparticles to fully expand and mature, forming microspheres with a stable size distribution suitable for subsequent applications.

The expansion of temperature-responsive microspheres was primarily due to the vaporization of the alkane core, which generated internal pressure, causing the microspheres to expand. Different alkanes had varying boiling points, leading to distinct expansion response and peak temperatures for each microsphere formulation. This experiment examined temperature-responsive microspheres with varying expansion response temperatures by incorporating different alkanes (Table 2).

As the temperature gradually rose, the expansion order of the microspheres was directly related to the boiling points of the contained alkanes. The lower the boiling point, the earlier the vaporization and expansion occurred. Specifically, microspheres with lower boiling-point alkanes began to vaporize and

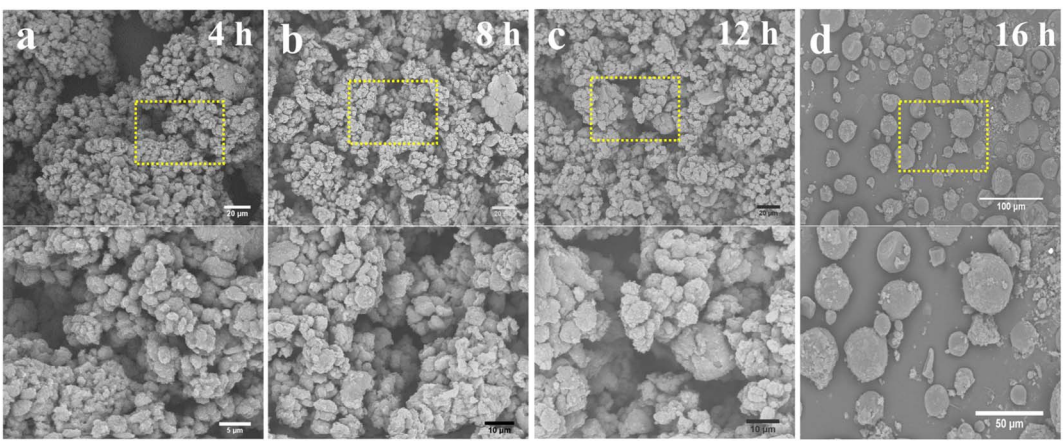

Fig. 4 (a–d) SEM images of temperature-responsive microspheres prepared with different reaction times.

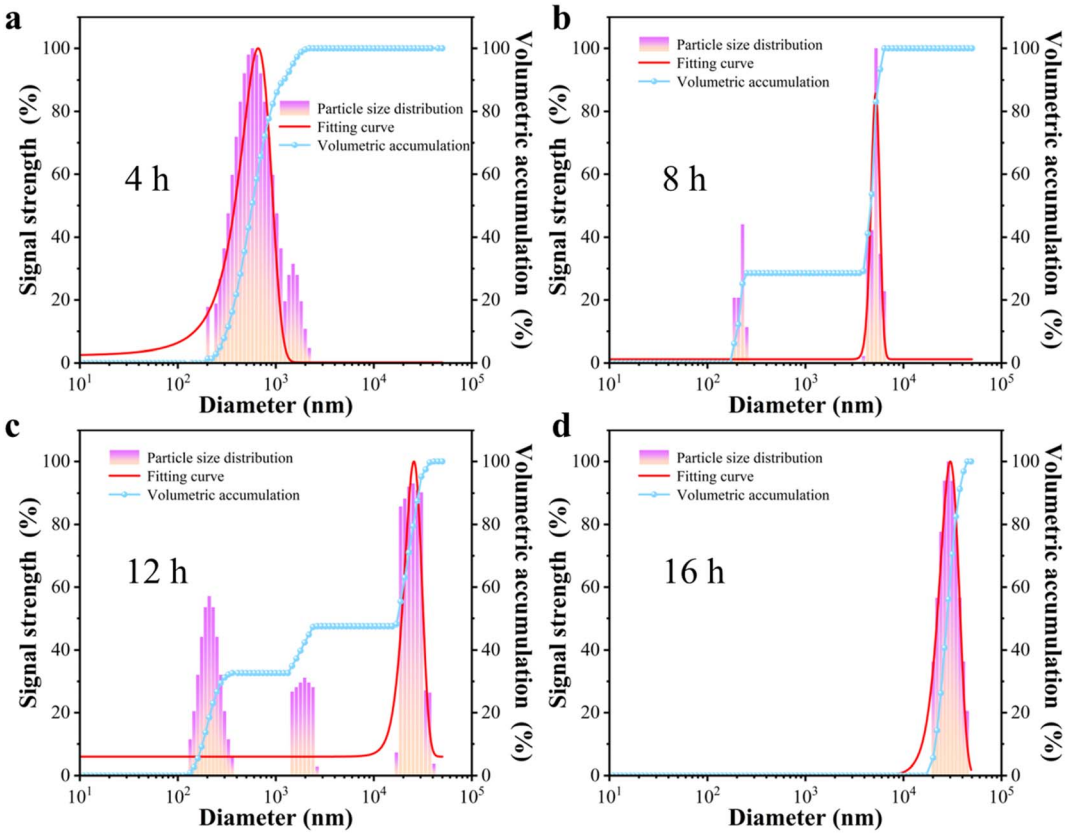

Fig. 5 (a–d) Particle size distribution at different times during the preparation of temperature-responsive microspheres.

Table 2 Temperature-responsive microspheres using different kinds of cores and their boiling points (the remaining conditions are the same as for TRM-1)

Sample	Core	Boiling point (°C)
TRM-6	*n*-Heptane	98
TRM-7	*n*-Octane	125–127
TRM-8	*n*-Nonane	151
TRM-9	*n*-Decane	174

expanded at lower temperatures. In contrast, as the boiling point increased, both vaporization and expansion temperatures rose. Therefore, temperature-responsive microspheres with a range of expansion temperatures could be designed to suit diverse application needs by precisely controlling the boiling points of the alkanes. As shown in Fig. S2,† the TRM-6 formulation containing *n*-heptane (boiling point: 98 °C) began to expand at approximately 100 °C. With further increases in temperature, *n*-heptane continued to vaporize, causing the microsphere volume to increase until it peaked at 180 °C. TRM-7, which contained *n*-octane (boiling point: 125–127 °C), started expanding around 130 °C, reaching its maximum volume at 180 °C. TRM-8, with *n*-nonane (boiling point: 151 °C), began expanding at 140 °C, with peak volume reached at 220 °C. In contrast, TRM-9, containing *n*-decane with a higher-boiling-point of 174 °C, started expanding at about 160 °C and peaked at 200 °C.

The possible expansion mechanism of the temperature-responsive microspheres was shown in Fig. S6.† During the heating process, the polymer became highly elastic when the temperature exceeded the glass transition temperature. Meanwhile, when the temperature exceeded the boiling point of alkanes, the pressure generated by alkane gasification caused the volume of microspheres to expand. By adjusting the alkane type and corresponding boiling point, different microsphere formulations could be designed for specific temperature ranges. For example, microspheres with low-boiling-point alkanes were suited for rapid expansion in low-temperature environments, while those with high-boiling-point alkanes provided stable expansion in high-temperature conditions. This approach allowed the optimization of alkane types and microsphere formulations to enhance performance across various applications. Fig. 6 showed that all temperature-responsive microspheres in Table 2 expanded successfully but exhibited distinct behaviors at different temperatures. The TRM-6 formulation with low-boiling-point *n*-heptane (98 °C) showed a tendency for overexpansion at high temperatures. As the temperature rose further, the pressure within the microspheres increased rapidly, exceeding the shell's structural limits and causing rupture. Due to its lower boiling point, *n*-heptane microspheres began expanding at lower temperatures but could surpass the physical limits at higher temperatures. In contrast,

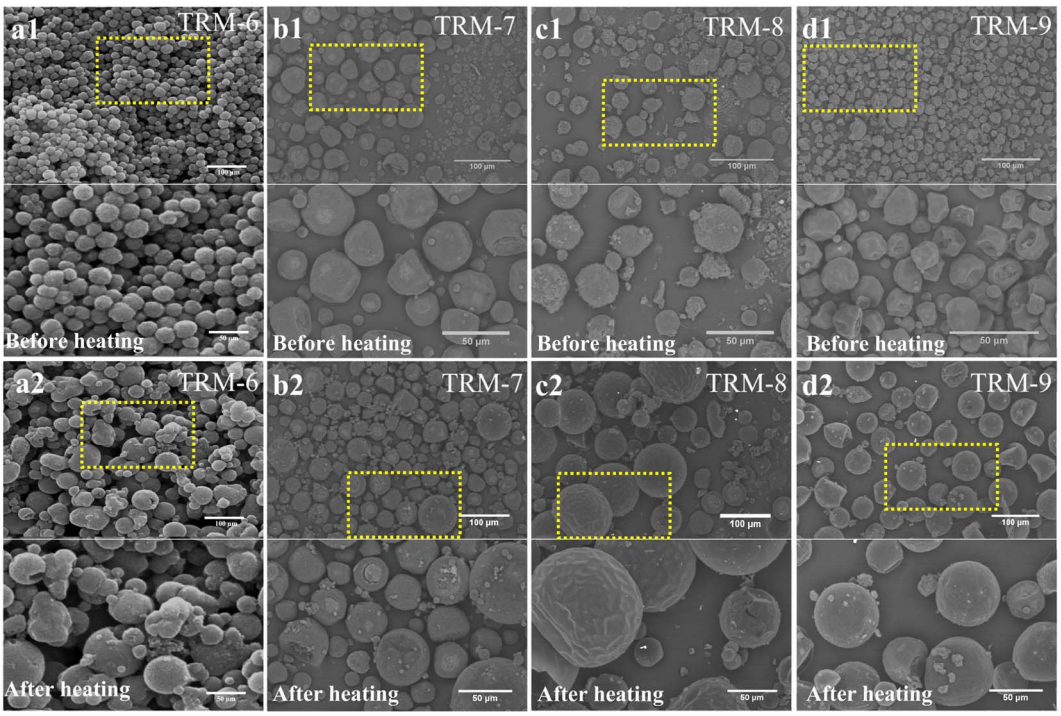

Fig. 6 (a1–d1) SEM images of temperature-responsive microspheres before heating. (a2–d2) SEM images of temperature-responsive microspheres after heating.

TRM-7, which contained *n*-octane (125–127 °C), underwent a milder expansion process, although some microspheres still ruptured under excessive internal pressure at higher temperatures. While TRM-7 showed less rupture than TRM-6, stability issues remained. TRM-8, containing *n*-nonane (151 °C), fell between TRM-7 and TRM-9 in behavior, with fewer ruptures and better thermal stability. After cooling, TRM-8 microspheres exhibited surface wrinkles, but with minimal shrinkage, showing good structural retention. TRM-9, containing higher-boiling-point *n*-decane (174 °C), demonstrated the highest heat resistance. These microspheres did not rupture during heating and maintained structural integrity even at high temperatures. However, some shrinkage occurred and created surface wrinkles during cooling, indicating that the cooling phase affected the microsphere structure.

DSC curves of TRM-6 to TRM-9 was shown in Fig. S3† and the enthalpies of phase transitions and their phase transition temperatures was presented in Table S1.† The results indicated that TRM-6 to TRM-9 underwent phase transition at different temperatures and the enthalpies of phase transitions were 21.149, 37.538, 37.028 and 26.996 J g^{-1}, respectively. This meant that the phase transition of the core led to the expansion of the microsphere volume, which was consistent with previous results.

To further investigate the expansion and thermal stability of the temperature-responsive microspheres from Table 2, thermogravimetric analysis was conducted on TRM-6, TRM-7, and TRM-9. As shown in Fig. 7, variations in core material types and boiling points resulted in distinct response temperatures. The boiling point of each core material directly influenced the onset

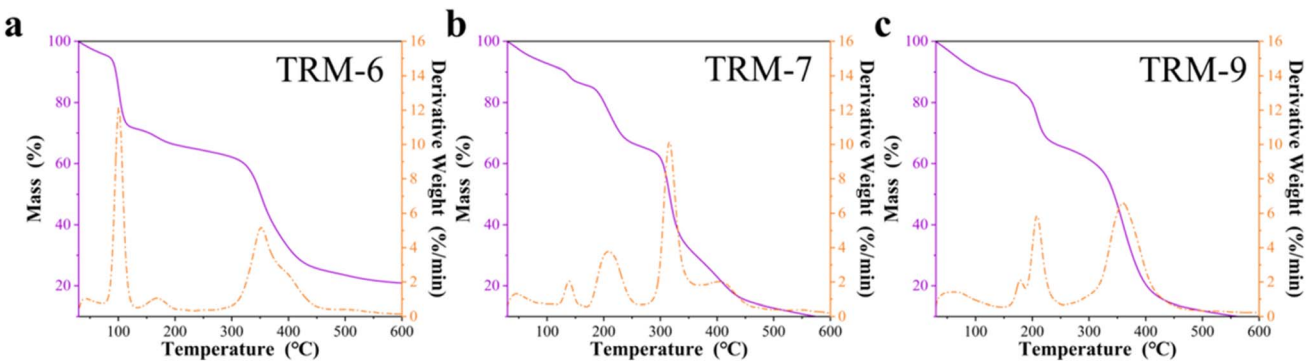

Fig. 7 (a–c) TG and DTG curves of TRM-6, TRM-7 and TRM-9.

temperature of microsphere expansion. For TRM-6, with a low-boiling-point core (*n*-heptane, approximately 100 °C), the expansion began at 100 °C, marked by a significant weight loss as the core material was released. This result indicated that TRM-6's temperature response was triggered at a lower temperature, allowing early-stage core release. In comparison, TRM-7, with a higher-boiling-point core (*n*-octane), began expanding around 150 °C, indicating a delayed temperature response and requiring a higher temperature to initiate the internal phase change and expansion. This result reflected that higher boiling points could effectively delay the microsphere response temperature, maintaining stability at elevated temperatures. TRM-9, with the highest boiling-point core (*n*-decane), only began expanding at 200 °C, which was later than TRM-6 and TRM-7, demonstrating enhanced thermal stability. TRM-9 retained structural integrity longer, only expanding significantly above 200 °C, making it particularly suitable for high-heat applications. Notably, all microspheres started decomposing at around 300 °C, confirming good thermal stability under high-temperature conditions. Even after exceeding their expansion points, TRM-6, TRM-7, and TRM-9 microspheres maintained structural stability until higher temperatures were reached where thermal decomposition occurred.

4. Conclusion

In this study, a temperature-responsive microsphere (TRM) with excellent expansion properties was prepared successfully by systematically optimizing formulation, reaction conditions, and polymerization time. Among the formulations tested, TRM-1 demonstrated the best morphological stability and expansion performance. The optimized conditions involving 1 g nano-SiO_2 (as a dispersant), 2 g SDS (as an emulsifier), 5 g ST, 5 g MA, 3 g MAA, 7 g MMA, and 0.43 g AIBN (as an initiator), with a 16-hour reaction at 65 °C, enabled the production of microspheres with stable spherical structures, high expansion ratios, and smooth, defect-free surfaces. In contrast, other formulations exhibited higher rates of rupture and shrinkage, suggesting lower structural stability. Furthermore, the polymerization time was found to influence particle size and structural maturity significantly, with a 16-hour duration yielding optimal expansion and consistent particle size distribution. In addition, it was possible to tailor the response temperature of the TRM to suit specific application needs by selecting different core materials. Overall, this work provided valuable insights for the development and optimization of temperature-responsive materials, supporting the potential use in a wide range of applications, including lightweight materials, phase-change materials, and the textile industry.

Data availability

The data that support the findings of this study are available from the corresponding author upon reasonable request.

Conflicts of interest

The authors declare no competing financial interest.

Acknowledgements

Dr Peng Xiao thanks the project support from State Grid Jiangsu Electric Power Co., Ltd (J2024106).

References

1 X. X. Zhang, Y. F. Fan, X. M. Tao and K. L. Yick, Fabrication and properties of microcapsules and nanocapsules containing n-octadecane, *Mater. Chem. Phys.*, 2004, **88**(2), 300–307.
2 Y. Kawaguchi, D. Ito, Y. Kosaka, M. Okudo, T. Nakachi, H. Kake, J. K. Kim, H. Shikuma and M. Ohshima, Thermally expandable microcapsules for polymer foaming—Relationship between expandability and viscoelasticity, *Polym. Eng. Sci.*, 2010, **50**(4), 835–842.
3 S. Jiao, Z. Sun, Y. Zhou, F. Li, J. Wen, Y. Chen, X. Du, L. Li and Y. Liu, Surface-Coated Thermally Expandable Microspheres with a Composite of Polydisperse Graphene Oxide Sheets, *Chem.–Asian J.*, 2019, **14**(23), 4328–4336.
4 Y. Xiao, Y. Xu, W. Wang, S. Yin, W. Zhao, R. Wei and C. Zhao, One-step engineering dual-network reinforced hydrogel microspheres with excellent anti-coagulant and low-density lipoprotein removal, *Sep. Purif. Technol.*, 2024, **331**, 125668.
5 X. Hong, B. Zhang, X. Zhang, Y. Wu, T. Wang and J. Qiu, Tailoring the structure and property of microfiltration carbon membranes by polyacrylonitrile-based microspheres for oil-water emulsion separation, *J. Water Proc. Eng.*, 2019, **32**, 100973.
6 B. T. Lobel, D. Baiocco, M. Al-Sharabi, A. F. Routh, Z. Zhang and O. J. Cayre, Current Challenges in Microcapsule Designs and Microencapsulation Processes: A Review, *ACS Appl. Mater. Interfaces*, 2024, **16**(31), 40326–40355.
7 T. He, X. Xu, B. Ni, H. Lin, C. Li, W. Hu and X. Wang, Metal–Organic Framework Based Microcapsules, *Angew. Chem., Int. Ed.*, 2018, **57**(32), 10148–10152.
8 T. Bollhorst, K. Rezwan and M. Maas, Colloidal capsules: nano- and microcapsules with colloidal particle shells, *Chem. Soc. Rev.*, 2017, **46**(8), 2091–2126.
9 J. G. Kim, J. U. Ha, S. K. Jeoung, K. Lee, S.-H. Baeck and S. E. Shim, Halloysite nanotubes as a stabilizer: fabrication of thermally expandable microcapsules *via* Pickering suspension polymerization, *Colloid Polym. Sci.*, 2015, **293**(12), 3595–3602.
10 S. K. Jeoung, I. S. Han, Y. J. Jung, S. Hong, S. E. Shim, Y. J. Hwang, P.-C. Lee and J. U. Ha, Fabrication of thermally expandable core–shell microcapsules using organic and inorganic stabilizers and their application, *J. Appl. Polym. Sci.*, 2016, **133**(47), 44247.
11 F. Lanza, A. J. Hall, B. Sellergren, A. Bereczki, G. Horvai, S. Bayoudh, P. A. G. Cormack and D. C. Sherrington, Development of a semiautomated procedure for the synthesis and evaluation of molecularly imprinted polymers applied to the search for functional monomers for phenytoin and nifedipine, *Anal. Chim. Acta*, 2001, **435**(1), 91–106.

12 L. Andersson and L. Bergström, Gas-filled microspheres as an expandable sacrificial template for direct casting of complex-shaped macroporous ceramics, *J. Eur. Ceram. Soc.*, 2008, **28**(15), 2815–2821.
13 M. J. Rheem, H. Jung, J. Ha, S.-H. Baeck and S. E. Shim, Suspension polymerization of thermally expandable microspheres using low-temperature initiators, *Colloid Polym. Sci.*, 2017, **295**(1), 171–180.
14 J. Hu, Z. Zheng, F. Wang, W. Tu and L. Lin, Synthesis and characterisation of thermally expandable microcapsules by suspension polymerisation, *Pigm. Resin Technol.*, 2009, **38**(5), 280–284.
15 S.-Y. Chen, Z.-C. Sun, L.-H. Li, Y.-H. Xiao and Y.-M. Yu, Preparation and characterization of conducting polymer-coated thermally expandable microspheres, *Chin. Chem. Lett.*, 2017, **28**(3), 658–662.
16 S.-Z. Jiao, Z.-C. Sun, F.-R. Li, M.-J. Yan, M.-J. Cao, D.-S. Li, Y. Liu and L.-H. Li, Preparation and Application of Conductive Polyaniline-Coated Thermally Expandable Microspheres, *Polymers*, 2019, **11**(1), 22.
17 M. Jonsson, O. Nordin, A. L. Kron and E. Malmström, Thermally expandable microspheres with excellent expansion characteristics at high temperature, *J. Appl. Polym. Sci.*, 2010, **117**(1), 384–392.
18 J. Cheng, M. Kang, Y. Liu, S. Niu, Y. Guan, W. Qu and S. Li, The preparation and characterization of thermal expansion capric acid microcapsules for controlling temperature, *Energy*, 2022, **261**, 125296.
19 M.-X. Liu, L.-H. Gan, W. Xiong, D.-Z. Zhu, Z.-J. Xu and L.-W. Chen, Partially graphitic micro- and mesoporous carbon microspheres for supercapacitors, *Chin. Chem. Lett.*, 2013, **24**(12), 1037–1040.
20 S. A. Odom, S. Chayanupatkul, B. J. Blaiszik, O. Zhao, A. C. Jackson, P. V. Braun, N. R. Sottos, S. R. White and J. S. Moore, A Self-healing Conductive Ink, *Adv. Mater.*, 2012, **24**(19), 2578–2581.
21 Y. Lu, J. Broughton and P. Winfield, A review of innovations in disbonding techniques for repair and recycling of automotive vehicles, *Int. J. Adhes. Adhes.*, 2014, **50**, 119–127.
22 L. Wei, S. Shang, Y. Zheng, J. Liu and P. Zhu, Iridescent structural colors printing on cellulose fabrics with robust structural coloration, *Dyes Pigm.*, 2024, **221**, 111824.
23 L. Wei, G. Lin, J. Liu, N. Lv, W. Jiang, C. Dong and S. Shang, Conductive Structural Colored Cotton Fabrics with Nonangle-Dependent Colors and Dynamic Thermal Management, *ACS Appl. Mater. Interfaces*, 2025, **17**(14), 21985–21995.
24 J. Wang, H. Xie, Z. Weng, T. Senthil and L. Wu, A novel approach to improve mechanical properties of parts fabricated by fused deposition modeling, *Mater. Des.*, 2016, **105**, 152–159.
25 A. R. Pak, J. H. Park and S. G. Lee, Blowing Properties and Functionality of Thermoplastic Polyester Film Using Thermally Expandable Microcapsules, *Polymers*, 2019, **11**(10), 1652.
26 Y. Wang, A. Gu, Z. Wei, Z. Zhao, H. Cong and C. Yan, Magnetic-induced dynamically enhanced in-plane or out-of-plane thermal conductivity of BN/Ag NWs@Ni/epoxy composites, *Ceram. Interfaces*, 2023, **49**(18), 30248–30256.
27 H.-M. Cong, Z.-B. Zhao, Y. Wang, X.-D. Yang, Y. Fang and C. Yan, A high thermal conductive BN-ZnO NWs/PVA composite based on the oriented structure construction using ice template method, *Ceram. Interfaces*, 2024, **50**(6), 8961–8970.
28 Y. Wang, Z. Zhao, A. Gu, Z. Wei, W. Chen and C. Yan, Enhancement of thermal conductivity of BN-Ni/epoxy resin composites through the orientation of BN-Ni fillers by magnetic field and hot-pressing, *Ceram. Interfaces*, 2022, **48**(22), 33571–33579.
29 X. Yang, Y. Fang, H. Cong, Z. Zhao, C. Yan and Y. Wang, Flexible BNOH@ polyurethane composites with high in-plane thermal conductivity for efficient thermal management, *J. Mater. Sci.*, 2024, **59**(19), 8220–8234.
30 Y. Wang, Y. Fang, X. Yang, H. Cong, Z. Zhao and C. Yan, Enhanced thermal conductivity and mechanical properties of boron nitride@polymethylacrylimide/epoxy composites with self-assembled stable three-dimensional network, *Chin. J. Chem. Eng.*, 2024, **75**, 230–238.
31 X. Yang, Y. Wang, H. Cong, Y. Fang, S. Chen, C. Yan and H. Deng, Construction of tree-ring mimetic 3D networks in polyvinyl alcohol/boron nitride composites for enhanced thermal management and mechanical properties, *Polymer*, 2024, **311**, 127531.
32 Y. Zheng, G. Lin, W. Zhou, L. Wei, J. Liu, S. Shang and P. Zhu, Bioinspired Polydopamine Modification for Interface Compatibility of PDMS-Based Responsive Structurally Colored Textiles, *ACS Appl. Mater. Interfaces*, 2024, **16**(38), 51748–51756.
33 C. Liang, Y. Jia, H. Qi, M. Chen, Y. Huang and W. Yang, From Cauliflowers to Microspheres: Particle Growth Mechanism in Self-Stabilized Precipitation Polymerization, *J. Phys. Chem. B*, 2024, **128**(31), 7673–7680.
34 W.-j. Liu, Y.-f. Cheng, X.-r. Meng, H.-h. Ma, C.-m. Shu, H. Fang, S.-x. Song and Z.-w. Shen, Synthesis of multicore energetic hollow microspheres with an improved suspension polymerization-thermal expansion method, *Powder Technol.*, 2019, **343**, 326–329.
35 L. J. Ji, Y. S. Jiang, G. Liang, Z. Q. Liu, J. Zhu, K. Huang and A. P. Zhu, Thermally expandable microspheres of poly (acrylonitrile/ethyl methacrylate/methacrylic acid) with fast thermal response property, *Pigm. Resin Technol.*, 2017, **46**(2), 115–121.
36 Z.-S. Hou and C.-Y. Kan, Preparation and properties of thermoexpandable polymeric microspheres, *Chin. Chem. Lett.*, 2014, **25**(9), 1279–1281.
37 Z. Hou, Y. Xia, W. Qu and C. Kan, Preparation and Properties of Thermoplastic Expandable Microspheres With P(VDC-AN-MMA) Shell by Suspension Polymerization, *Int. J. Polym. Mater. Polym. Biomater.*, 2015, **64**(8), 427–431.
38 Y. Xu, Q. Liu, J. Zhu, H. Zhang, J. Liu, R. Chen, J. Yu, G. Sun and J. Wang, Self-assembled porous polydopamine microspheres modified polyacrylonitrile fiber for synergistically enhanced U(VI) extraction and seawater desalination, *Sep. Purif. Technol.*, 2023, **306**, 122684.

39 Y.-F. Xu, M.-Z. Wang, Q.-C. Wu, X. Zhou and X.-W. Ge, Synthesis and morphology control of raspberry-like poly(ethylene terephthalate)/polyacrylonitrile microspheres, *Chin. Chem. Lett.*, 2016, **27**(2), 195–199.

40 H. Zhang, L. Xu, F. Yang and L. Geng, The synthesis of polyacrylonitrile/carbon nanotube microspheres by aqueous deposition polymerization under ultrasonication, *Carbon*, 2010, **48**(3), 688–695.

41 J. Zhang, Y. Zhou, B. Huang, S. Lv, X. Ma and J. Tang, Synthesis and characterization of high temperature resistant thermal expansion microsopheres with P(acrylonitrile/methacrylic acid/N,N-dimethylacrylamide/n-butylacrylate) shell, *SN Appl. Sci.*, 2019, **1**(8), 923.

42 W. Zhao, L. Duan, B. Zhang, X. Ren and G. H. Gao, Tough and ultrastretchable hydrogels reinforced by poly(butyl acrylate-co-acrylonitrile) latex microspheres as crosslinking centers for hydrophobic association, *Polymer*, 2017, **112**, 333–341.

43 D. Hulicova, K. Hosoi, S.-i. Kuroda and A. Oya, Carbon nanotubes prepared from three-layered copolymer microspheres of acrylonitrile and methylmethacrylate, *Carbon*, 2005, **43**(6), 1246–1253.

44 N. N. S. Subri, P. A. G. Cormack, S. N. A. Md. Jamil, L. C. Abdullah and R. Daik, Synthesis of poly(acrylonitrile-co-divinylbenzene-co-vinylbenzyl chloride)-derived hypercrosslinked polymer microspheres and a preliminary evaluation of their potential for the solid-phase capture of pharmaceuticals, *J. Appl. Polym. Sci.*, 2018, **135**(2), 45677.

45 S. Zhou, Z. Zhou, W. Xu, H. Ma, F. Ren and H. Shen, Water as Blowing Agent: Preparation of Environmental Thermally Expandable Microspheres *via* Inverse Suspension Polymerization, *Polym.-Plast. Technol. Eng.*, 2018, **57**(10), 1026–1034.

46 W. Han, S. Dong, B. Li and L. Ge, Preparation of polyacrylonitrile- based porous hollow carbon microspheres, *Colloids Surf., A*, 2017, **520**, 467–476.

47 K. Trangwachirachai and Y.-C. Lin, Light hydrocarbon conversion to acrylonitrile and acetonitrile – a review, *Dalton Trans.*, 2023, **52**(19), 6211–6225.

48 Y. Gao, N. Zhang, L. Zhu and Z. Hou, Preparation and Properties of Thermoplastic Expandable Microspheres with P(AN-MMA) Shell, *Russ. J. Appl. Chem.*, 2017, **90**(10), 1634–1639.

49 H. T. Kim, A. K. Jaladi, Y. J. Lee and D. K. An, Thermal Expansion Behavior of Thermally Expandable Microspheres Prepared by Suspension Polymerization Using P(AN-MMA-MAA) Core/Shell, *Bull. Korean Chem. Soc.*, 2020, **41**(2), 190–195.

50 K. Xu, X. Zhao, J. Yu, Q. Nong and H. Qian, Preparation of poly(acrylonitrile-co-styrene) microspheres by reflux precipitation polymerization, *J. Macromol. Sci., Part A:Pure Appl. Chem.*, 2024, **61**(10), 742–751.

51 G. Xie, Z. Wang and Y. Bao, Expansion Properties and Diffusion of Blowing Agent for Vinylidene Chloride Copolymer Thermally Expandable Microspheres, *Materials*, 2020, **13**(17), 3673.

52 G. Xie, P. Pan and Y. Bao, Morphology and blowing agent encapsulation efficiency of vinylidene chloride copolymer microspheres synthesized by suspension polymerization in the presence of a blowing agent, *J. Appl. Polym. Sci.*, 2017, **134**(4), 44376.

53 Q. Yi, J. Li, R. Zhang, E. Ma and R. Liu, Preparation of small particle diameter thermally expandable microspheres under atmospheric pressure for potential utilization in wood, *J. Appl. Polym. Sci.*, 2021, **138**(4), 49734.

54 S. He, H. Yuan and X. Yang, Preparation of Double-Layer Hollow Porous Carbon Microspheres by a Hydrothermal Method, *ChemistrySelect*, 2023, **8**(29), e202301752.